Collective Drifts in Vibrated Granular Packings: The Interplay of Friction and Structure

A. Plati[1,2] and A. Puglisi[1,2,3]
[1]Department of Physics, University of Rome Sapienza, Piazzale Aldo Moro 2, 00185 Rome, Italy
[2]Institute for Complex Systems—CNR, Piazzale Aldo Moro 2, 00185 Rome, Italy
[3]INFN, University of Rome Tor Vergata, Via della Ricerca Scientifica 1, 00133 Rome, Italy

(Received 13 October 2021; revised 18 February 2022; accepted 4 April 2022; published 17 May 2022)

We simulate vertically shaken dense granular packings with horizontal periodic boundary conditions. A coordinated translating motion of the whole medium emerges when the horizontal symmetry is broken by disorder or defects in the packing and the shaking is weak enough to conserve the structure. We argue that such a drift originates in the interplay between structural symmetry breaking and frictional forces transmitted by the vibrating plate. A nonlinear ratchet model with stick slips reproduces many faces of the phenomenon. The collective motion discussed here underlies phenomena observed recently with vibrofluidized granular materials, such as persistent rotations and anomalous diffusion.

DOI: 10.1103/PhysRevLett.128.208001

Introduction.—One of the major challenges of statistical mechanics, nowadays, is understanding systems far from equilibrium, e.g., in the presence of energy flows or dissipation [1]. A realm of physics where fluctuations and lack of thermodynamic equilibrium are ubiquitous is soft matter [2] and, in this context, an established test ground for theories is provided by vibrofluidized granular systems [3–6] where energy is continuously injected from an external source and dissipated in friction. When isotropy is broken, a fraction of this energy current can be exploited to realize a ratchet effect [7–12] similar to what is seen in active matter [13]. A series of recent granular experiments suggests that spontaneous persistent drifts emerge in the presence of isotropic disorder: this is revealed by superdiffusion [14], which has been connected to transient drifts with very long relaxation times [15,16], or by the appearance of steady rotations of disks in dense vibrated packings [17] and by the emergence of collective motions under swirling excitations [18,19]. In all these examples random energy is converted into a steady flow, realizing an interesting class of "disordered engines."

Here we aim at understanding the general ingredients underlying these effects, focusing on a few simplified setups and—in the conclusions—on a model of frictional ratchet. The mechanism investigated explains the aforementioned phenomena as it represents their translational (instead of rotational) [14–16], collective (instead of individual) [17], and spontaneous (instead of externally stimulated) [18,19] counterpart.

Numerical setup.—We simulate, through an established discrete elements method, a system of N spherical grains confined by hard walls and/or periodic boundary conditions (PBC) with different geometries. Each grain has radius R_i, mass m_i, position $r_{\alpha i}$, velocity $v_{\alpha i}$, and angular velocity $\omega_{\alpha i}$, where $\alpha = \{x, y, z\}$ and $i = \{1, \ldots, N\}$. The grain-grain and grain-boundary contact forces follow the Hertz Mindlin model; see details in the Supplemental Material [20]. In all cases the setup is enclosed in a 3D box of height $10 \times 2\max_i R_i$, energy is injected by vertical vibrations $z(t) = A\cos(2\pi f t)$ of the upper and lower confining hard walls, and there is one or more horizontal direction with infinite horizon (i.e., where movement is not constrained by walls). In quasi-2D setups [cases in Figs. 1(a)–1(g), $N = 60$] x has PBC while y is confined by two parallel vertical walls of width $L = 32$ mm separated by a distance $d = 2\max_i R_i$. In the full 3D case in Fig. 1(h) ($N = 2600$) both x and y directions have PBC, and the base of the box has dimensions 98×98 mm^2. In the full 3D case in Fig. 1(i)

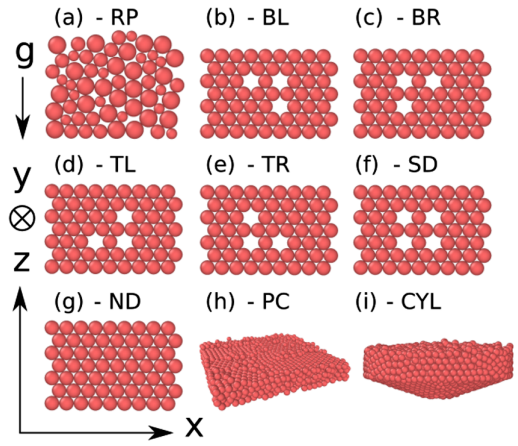

FIG. 1. Simulation geometries. Quasi 2D vertical layers can be random polydisperse (a)—with equal proportions of three species of radii $R_i = \{1.5, 2.0, 2.5\}$ mm—or ordered monodisperse (b)–(g)—$R_i = R = 2$ mm—with, eventually, defects. The defect nomenclature is related to the position of the grain that breaks the symmetry. The 3D setups are a cubic (h) and cone-base cylinder (i) (see Ref. [15] for details), both monodisperse.

($N = 2600$) the box is a cylinder with a conical-shaped base, identical to what was previously used in experiments and simulations [14–16]. The shaking intensity is measured by $\Gamma = A(2\pi f)^2/g$, where g is the gravity acceleration. Here we always vary Γ by A keeping f constant at 100 Hz in the quasi-2D simulation and at 200 Hz in the all other ones.

Regarding the quasi-2D setups, we prepare the initial state of our packings in two main ways: The first one consists of randomly pouring a polydisperse assembly of grains in the container; initial velocities are zero, but during the pouring dynamics they acquire energy and rapidly reach a stationary statistics. The second one is obtained by placing a monodisperse assembly on a hexagonal lattice with the possibility to have vacancies in determined sites, while the particles' initial velocities are drawn from a Gaussian distribution with zero mean and a variance small enough to keep the crystal stable. For the 3D cases we simply pour monodisperse grains in the containers. Since the latter do not satisfy the right proportions for crystallization the resulting packings are fairly disordered. The monodisperse packings with quasi-2D geometry [Figs. 1(b)–1(g)] can be without defects [Fig. 1(g)], or with four symmetric defects [Fig. 1(f)], or with three defects placed to break in different ways the symmetry of the crystal with respect to z and x [Figs. 1(b)–1(e)]. The polydisperse quasi-2D packing [Fig. 1(a)] is inspired by a recent experimental and numerical study [17] with shaken disks without PBC: for Γ low enough a persistent net angular velocity is seen for each disk. We verified (see the Supplemental Material [20]) that such persistent rotational modes are present also in our simulations with spheres, in all the geometries explored here, with both hard walls and PBC. However, in this Letter, we focus on simulations with horizontal PBC only, where a different phenomenon, namely the collective horizontal persistent drift, superimposed on the previously observed rotational modes, appears.

Drifting disordered packings.—We start from polydisperse packings in the quasi-2D geometry. At low values of Γ all of the system moves coherently with the center of mass (c.m.) along the x axis, i.e., the free direction allowed by PBC, whose motion in time $X^{\mathrm{c.m.}}(t) = M_{\mathrm{tot}}^{-1}\sum_i m_i x_i(t)$ is shown in Fig. 2(a). We note that, even with the same Γ, a different random packing can lead to a stable drift with very different magnitudes or to an intermittent drift. In Fig. 2(b), considering the x component of the c.m.'s velocity $V_x^{\mathrm{c.m.}}(t)$, we also verify that short time properties as the time variance $\sigma^2(V_x^{\mathrm{c.m.}})$ are fully determined by the driving parameters (small error bars), while the slow cooperative dynamics (characterized by its time average $\langle V_x^{\mathrm{c.m.}}\rangle$) sensibly depends on the packing configuration (large error bars). Nevertheless, raising Γ up to values for which the system fluidizes (typically $\Gamma > 10$), the c.m. performs Brownian-like trajectories and $\langle V_x^{\mathrm{c.m.}}\rangle$ vanishes (see the Supplemental Material, Video 1 [20]). We recall that a dense vibrofluidized granular

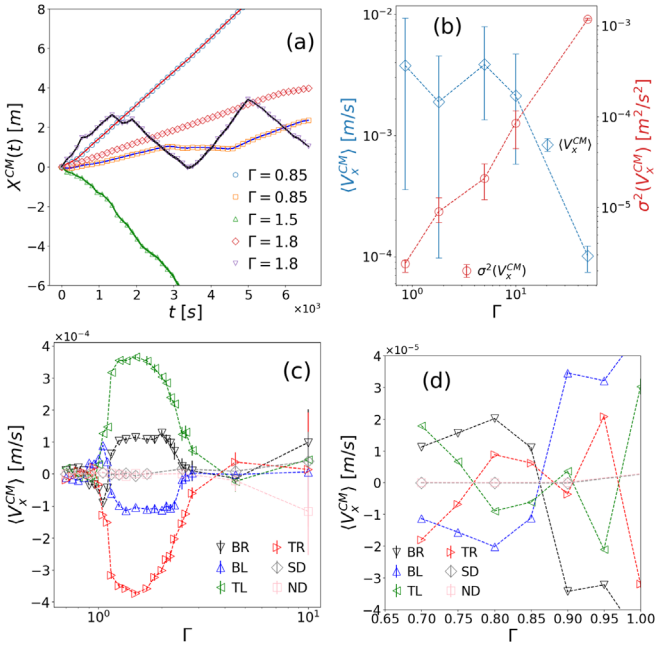

FIG. 2. (a) $X^{\mathrm{c.m.}}(t)$ (symbols) and $x_i(t)$ for all the grains i in the system (lines) for quasi-2D random packings. The grains move coherently with the c.m. Simulations with the same Γ refer to different random realizations. (b) Comparison between $\sigma^2(V_x^{\mathrm{c.m.}})$ and $\langle V_x^{\mathrm{c.m.}}\rangle$, obtained averaging over three independent random realizations. (c) Time averaged velocity of center of mass as a function of Γ for different monodispersed packings. Each point is mediated over five independent realizations of the dynamics. Here, differently from random packings, $\langle V_x^{\mathrm{c.m.}}\rangle$ vanishes for $\Gamma \simeq 3$ because moderate vibrations destroy the asymmetric configuration of defects. (d) enlargement of low Γs to highlight the sign changes with fixed structure.

system has several timescales, the smallest associated to fast vibrational motion, the largest associated to slow rearrangements of the global contact network. What we observe here is a rapid divergence of the largest timescale when Γ is reduced below $\sim 3 \div 10$. The value of $\langle V_x^{\mathrm{c.m.}}\rangle$, therefore, does not depend crucially on the trajectory's duration, provided it is longer than the small timescales, e.g., $\gg 10^{-1}$ s.

Effect of symmetries.—The observation that average motion is erased by fast particle rearrangements (fluidization) is a hint of its correlation with the system's spatial configuration. For this reason we study $\langle V_x^{\mathrm{c.m.}}\rangle$ for ordered packings with defects [Fig. 2(c)]. Net drifts are never observed in the ND and SD cases, whereas for all asymmetric configurations they are. Moreover, when the defect configuration is mirrored with respect to the z axis, e.g., BL → BR or TR → TL, etc., at a given value of Γ, $\langle V_x^{\mathrm{c.m.}}\rangle$ changes its sign remaining with comparable magnitude. A reflection of the configuration with respect to x always changes the magnitude of the drift, but the sign reverses just for a few values of Γ. Remarkably, a variation of Γ keeping the same layout of defects brings multiple inversions of $\mathrm{sgn}(\langle V_x^{\mathrm{c.m.}}\rangle)$ in the region $0.8 \leq \Gamma \leq 1.05$,

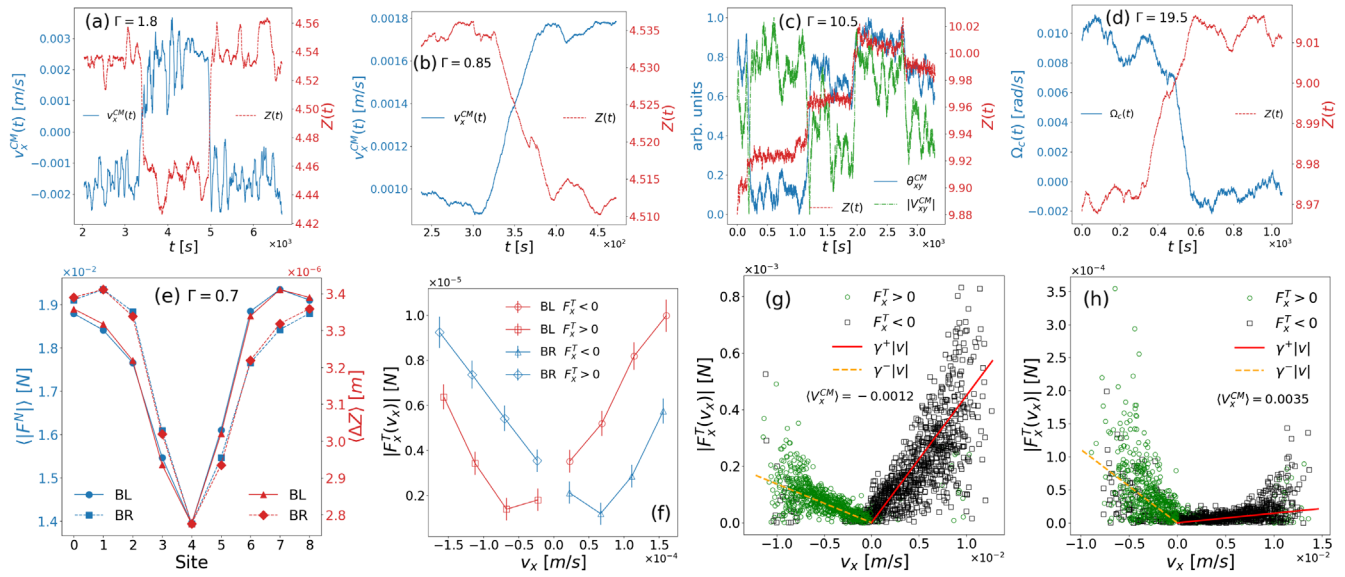

FIG. 3. (a)–(d) Comparison between the time evolution of the c.m. velocity and the mean coordination number of the contact network $Z(t) = N^{-1} \sum_{ij} \Theta(R_i + R_j + \delta - |\boldsymbol{r}_{ij}|)$ where $0 < \delta \ll R_i + R_j$ allows one to detect the nearest neighbor not in contact due to vibrations. Trajectories are smoothed with a running average. (a)–(b) random packings [cases with upside-down triangles and circles in Fig. 2(a)]. (c) 3D cubic setup. Here $V_{xy}^{\mathrm{c.m.}}$ is two-dimensional so we plot both the modulus and the orientation $\theta_{xy}^{\mathrm{c.m.}}$. (d) 3D cylindrical geometry. The collective motion is a rotation around the central axis so $\Omega_c = N^{-1} \sum_i |\boldsymbol{r}_i|^{-2} (\boldsymbol{r}_i \times \boldsymbol{v}_i)_z$. (e) Time averaged modulus of the normal force and compenetration between the plate and the bottom particles for two z-reflected configurations of defects. Site four is under the double defect [see Figs. 1(b)–1(c)]. (f)–(h) Scatter plots with bins of the total x-tangential force modulus exerted by the plate vs the total velocity of the bottom particles for ordered packings with defects (f) and random packings (g)–(h) shaken at $\Gamma = 0.7$. In the latter, $\gamma^{\pm} = |\langle F_x^T | v_x \gtrless 0 \rangle| / \langle v_x | v_x \gtrless 0 \rangle$ linearly interpolate the data clouds.

shown enlarged in Fig. 2(d). In summary, (i) defect asymmetry is needed to observe nonzero mean velocity of the c.m., (ii) reflection with respect to z inverts the direction of motion, and (iii) the defect configuration alone does not define the verse of the motion; the driving parameter determines it too (Supplemental Material, Video 2 [20]).

Sensitivity to small configuration changes.—Given the observed complicated entanglement of external parameters and drifts, we now focus on fluctuations of the drift during the same trajectory. Such fluctuations are more evident and frequent in random packings. Figures 3(a) and 3(b) compare the coordination number of the contact network $Z(t)$ with the instantaneous drift $V_x^{\mathrm{c.m.}}(t)$: they often change together. Such changes do not correspond to a significant rearrangement of particles [changes of $Z(t)$ can be smaller than 1%], confirming that the collective motion is sensible to small deformations of the contact network. Collective drifts are also observed in the 3D realistic setups (see Refs. [15,16] and the Supplemental Material [20]), and similar correlations are present here too [Figs. 3(c)–3(d)]. Obviously, the coordination number is not directly related to the packing asymmetry. A more appropriate quantity eluded our analysis, perhaps because of the observed challenging scenario: on one hand, the drift may significantly change at fixed Γ for weak deformations of the contact network (as seen for random packings) and, on the other hand, it can change direction by varying the driving parameters with a fixed structure (as occurs in the ordered packings with defects). Analogous difficulties have been discussed recently for glassy systems [34–39]. In our Letter, the athermal nature of the system (that needs a mechanical driving to reach a stationary state) is a peculiar feature that has no counterpart in thermal glasses [40].

Bulk asymmetries originate a ratchet effect.—We now look for observables that mediate between bulk structure and dynamics. The profiles, along x of the mean normal pressure and the mean compenetration between the plate and the bottom particles are shown in Fig. 3(e), for an ordered packing with defects. Each profile is asymmetric and properly inverted under a z reflection: defects in the bulk actually influence the way in which the boundaries interact with the source of energy. This may be expected, since both normal pressure and compenetration affect the tangential component of the force exerted by the vibrating plate (see the Supplemental Material [20]); what is remarkable in our opinion is its global dynamical consequence. Recent analytical results [41] for an idealized model of vibrofluidized dense granular material suggest long-range spatial correlations that may justify the global influence of defects. A deeper insight is provided by the external tangential force provided by the plate F_x^T (x component), which directly affects the c.m.: $\dot{V}_x^{\mathrm{c.m.}} = M_{\mathrm{tot}}^{-1} F_x^T(r_{xj}, r_{zj}, v_{xj}, \omega_{yj})$ where the index j refers to the

bottom particles (for ordered packings $j \in [1, 9]$). We characterize the dependence of F_x^T upon $v_x = \sum_j v_{xj}$ by the scatter plot in Fig. 3(f) for two z-reflected ordered configurations with defects. Such dependence is typical of a frictional force, but quite surprisingly, its intensity depends on the sign of the velocity. Moreover, also this frictional asymmetry is inverted under the z reflection of packing. Comparing with Fig. 2(d) clarifies that the drift occurs toward lower friction. Figures 3(g) and 3(h) show that the same kind of bias is more pronounced for random packings; indeed, $|\langle V_x^{\mathrm{c.m.}} \rangle|$ is far larger. All this makes clear that structural disorder and defects introduce an asymmetric interaction with the plate. The role of the ω_{yj} is discussed in the Supplemental Material [20].

Simulations with a higher acquisition rate allow one to study the grain trajectories on timescales shorter than a driving period $1/f$. In Fig. 4(a), we show $F_c(t) = \mu |F^N| - |F_x^T|$ where μ is the dynamic friction coefficient. As explained in the Supplemental Material [20], this difference is zero if the grain and the plate surfaces slide on each other. We observe roughly periodic cycles (with the periodicity of the driving plate), with a part of each period where $F_c \sim 0$. In Fig. 4(b), we compare the trajectory of the c.m. with the total horizontal displacement accumulated by the bottom layer considering just the sliding instants and all the remaining ones. From this comparison we conclude that the main contribution to the irreversible motion occurs when $F_c \sim 0$. From Fig. 4(c) we also understand how the mean horizontal motion originated at the bottom of the system is transferred to the top; there we plot the difference ΔX between the mean x coordinate of the lowest layer and of the one just above it, noting a clear stick-slip dynamics. We have verified that, as suggested by the marked points in the graph, this distance slowly increases during the sliding of the bottom layer and then suddenly decreases when the sliding condition ceases.

The provided analysis suggests the interpretation of the phenomenon under study as a ratchet effect originated from structural asymmetries [42,43]. To further support this, a variation of the well-known periodically rocked ratchet [44] is proposed in the Supplemental Material [20]. Inspired by the stick-slip dynamics between the layers of the granular packing we have replaced the asymmetric periodic potential with a confining but slipping one. Our model reproduces many features of the phenomenon under study (see the Supplemental Material [20]).

System's size effects.—The results for 2D packings are obtained in a relatively small system in order to establish a direct connection with former experiments [17]. The presence of analogous behavior also in larger and more realistic 3D systems signals the generality of the phenomenon. Nevertheless, a study of the system's size effects in the simplified geometry is nontrivial since the origin of the drift and the resistance against it can depend both on bulk volume (through the concentration of defects) and external surfaces (through friction and energy input). We performed simulations of ordered packings with defects where the

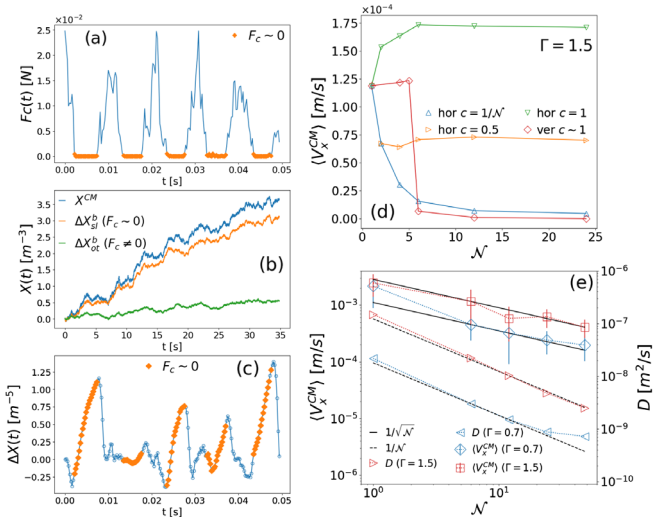

FIG. 4. (a) Time evolution of $F_c = \mu |F^N| - |F_x^T|$. Diamonds mark the instants for which $F_c \sim 0$ corresponding to the sliding condition for the tangential force between the plate and the bottom grains. (b) Trajectory of the $X^{\mathrm{c.m.}}$ compared with the horizontal displacement of the bottom layer accumulated in the sliding instants (ΔX^b_{sl}) and in all the other ones (ΔX^b_{ot}). (c) Stick slip in the difference of the mean x coordinates of the two lowest horizontal layers in a granular simulation. Diamonds refer to sliding instants. These three panels are obtained with BL and $\Gamma = 1.25$. (d) Mean velocity of the c.m. as a function of the horizontal (triangles) and vertical (diamonds) size of the system for different values of the defect concentration. The vertical size effect is shown for $c = 1$, but we verified that its relevant behavior does not depend on $c > 0$. (e) Scaling of $\langle V_x^{\mathrm{c.m.}} \rangle$ and the diffusivity of the fluctuation around the drift D (see the Supplemental Material [20]) as a function of the horizontal system size for random packings. Each point is obtained averaging over ten independent realizations of the packing; error bars are standard deviations.

original "module" of $N \sim 60$ grains is replicated $\mathcal{N}$ times along both the x or the z axis. Each replica can be with or without defects so that a concentration of defects c can be defined as the number of asymmetric modules over $\mathcal{N}$. For the horizontal size scaling we considered three different values of defect concentration $c = \{1/\mathcal{N}, 0.5, 1\}$. From Fig. 4(d) we see that increasing the system size along x with a vanishing concentration of defects ($c = 1/\mathcal{N}$) leads to the weakening of the drift. For finite defect concentration instead, we observe a nonzero-asymptotic $\langle V_x^{\mathrm{c.m.}} \rangle$ whose magnitude depends on c. Regarding the vertical size scaling, we note that the drift is suppressed for large $\mathcal{N}$. This fact can be reasonably explained considering that, in absence of a lateral wall in the x direction, the pressure at the base of the system increases with its height reducing the global mobility. We have accordingly verified that for packings higher than $\mathcal{N} = 5$, the sliding condition $\mu |F^N| \sim |F_x^T|$ is never satisfied. The scenario for large random packings is different: the global asymmetry of many

disordered granular patches each pushing the whole system in a different direction is expected to decrease with their number. Indeed we observe a reduction of the drift as $1/\sqrt{\mathcal{N}}$ when the system size is scaled horizontally [Fig. 4(e)]. Interestingly, also the diffusivity of the fluctuations around the average motion decreases with $\mathcal{N}$. We define such a quantity as the diffusion coefficient D of the fast component of the c.m. dynamics that can be measured from the power spectral density of $V_x^{\mathrm{c.m.}}(t)$ as shown in the Supplemental Material [20]. For $\Gamma > 1$ it follows a scaling $D \sim 1/\mathcal{N}$ while for $\Gamma < 1$ it seems to reach a minimum at large $\mathcal{N}$. In the former case the quantity $D/\langle V_x^{\mathrm{c.m.}}\rangle^2$ that is the typical time after which the drift (even very small) becomes visible is independent from $\mathcal{N}$. This observation confirms that the drift is more relevant than a finite-size effect and poses an interesting challenge for the recently discovered thermodynamic uncertainty relations [45,46].

Conclusion.—We have presented a numerical study of a realistic granular contact model with several ideal experiments to put in evidence the existence of a random-to-direct energy conversion based upon the concurrent breaking of time and space symmetries. As in many ratchetlike phenomena, the same geometry may lead to opposite drifts, depending on energy injection. Inspired by the interplay of friction and structure that emerged in the numerical analysis, we introduce a novel ratchet model with asymmetric interactions and stick slips. The drifts discovered and explained underlie several phenomena observed recently in shaken granular media [14–17] and are expected to be a general feature of soft matter systems, such as active matter, crowd dynamics, etc.

The authors are indebted to Marco Baldovin and Rafael Díaz Hernández Rojas for fruitful scientific discussions. The authors acknowledge the financial support from the MIUR PRIN2017 Project No. 201798CZLJ.

[1] U. M. B. Marconi, A. Puglisi, L. Rondoni, and A. Vulpiani, Phys. Rep. **461**, 111 (2008).
[2] S. R. Nagel, Rev. Mod. Phys. **89**, 025002 (2017).
[3] L. P. Kadanoff, Rev. Mod. Phys. **71**, 435 (1999).
[4] H. M. Jaeger, S. R. Nagel, and R. P. Behringer, Rev. Mod. Phys. **68**, 1259 (1996).
[5] M. Rodhes, *Principles of Powder Technology* (John Wiley and Sons, New York, 1997).
[6] L. de Arcangelis, E. Lippiello, M. Pica Ciamarra, and A. Sarracino, Phil. Trans. R. Soc. A **377**, 20170389 (2019).
[7] P. Reimann, Phys. Rep. **361**, 57 (2002).
[8] P. Hänggi and F. Marchesoni, Rev. Mod. Phys. **81**, 387 (2009).
[9] G. Costantini, U. Marini Bettolo Marconi, and A. Puglisi, Phys. Rev. E **75**, 061124 (2007).
[10] P. Eshuis, K. van der Weele, D. Lohse, and D. van der Meer, Phys. Rev. Lett. **104**, 248001 (2010).
[11] A. Gnoli, A. Petri, F. Dalton, G. Pontuale, G. Gradenigo, A. Sarracino, and A. Puglisi, Phys. Rev. Lett. **110**, 120601 (2013).
[12] R. Balzan, F. Dalton, V. Loreto, A. Petri, and G. Pontuale, Phys. Rev. E **83**, 031310 (2011).
[13] R. Di Leonardo, L. Angelani, D. Dell'Arciprete, G. Ruocco, V. Iebba, S. Schippa, M. P. Conte, F. Mecarini, F. De Angelis, and E. Di Fabrizio, Proc. Natl. Acad. Sci. U.S.A. **107**, 9541 (2010).
[14] C. Scalliet, A. Gnoli, A. Puglisi, and A. Vulpiani, Phys. Rev. Lett. **114**, 198001 (2015).
[15] A. Plati, A. Baldassarri, A. Gnoli, G. Gradenigo, and A. Puglisi, Phys. Rev. Lett. **123**, 038002 (2019).
[16] A. Plati and A. Puglisi, Phys. Rev. E **102**, 012908 (2020).
[17] C. F. Moukarzel, G. Peraza-Mues, and O. Carvente, Phys. Rev. Lett. **125**, 028001 (2020).
[18] S.-C. Zhao and T. Pöschel, Phys. Fluids **33**, 081701 (2021).
[19] S.-C. Zhao and T. Pöschel, Phys. Rev. E **105**, L022902 (2022).
[20] See Supplemental Material http://link.aps.org/supplemental/10.1103/PhysRevLett.128.208001 for more informations and additional numerical analysys, which includes Refs. [22–34].
[21] S. Plimpton, J. Comput. Phys. **117**, 1 (1995).
[22] http://lammps.sandia.gov/.
[23] H. P. Zhang and H. A. Makse, Phys. Rev. E **72**, 011301 (2005).
[24] L. E. Silbert, D. Ertaş, G. S. Grest, T. C. Halsey, D. Levine, and S. J. Plimpton, Phys. Rev. E **64**, 051302 (2001).
[25] N. V. Brilliantov, F. Spahn, J. M. Hertzsch, and T. Pöschel, Phys. Rev. E **53**, 5382 (1996).
[26] V. L. Popov, *Contact Mechanics and Friction* (Springer-Verlag, Berlin, 2010).
[27] https://docs.lammps.org/pair_granular.html.
[28] A. Di Renzo and F. P. Di Maio, Chem. Eng. Sci. **59**, 525 (2004).
[29] T. S. T. Pöschel, *Computational Granular Dynamics* (Springer, Berlin, 2005).
[30] M. Rackl and K. J. Hanley, Powder Technol. **307**, 73 (2017).
[31] A. Plati, L. de Arcangelis, A. Gnoli, E. Lippiello, A. Puglisi, and A. Sarracino, Phys. Rev. Research **3**, 013011 (2021).
[32] J. Wilkie, Phys. Rev. E **70**, 017701 (2004).
[33] A. Stukowski, Model. Simul. Mater. Sci. Eng. **18**, 015012 (2010).
[34] R. Díaz Hernández Rojas, G. Parisi, and F. Ricci-Tersenghi, Soft Matter **17**, 1056 (2021).
[35] C. Coulais, R. P. Behringer, and O. Dauchot, Soft Matter **10**, 1519 (2014).
[36] H. Tong and H. Tanaka, Phys. Rev. X **8**, 011041 (2018).
[37] E. D. Cubuk, S. S. Schoenholz, J. M. Rieser, B. D. Malone, J. Rottler, D. J. Durian, E. Kaxiras, and A. J. Liu, Phys. Rev. Lett. **114**, 108001 (2015).
[38] H. G. E. Hentschel, I. Procaccia, and S. Roy, Phys. Rev. E **100**, 042902 (2019).
[39] Z. Schwartzman-Nowik, E. Lerner, and E. Bouchbinder, Phys. Rev. E **99**, 060601(R) (2019).
[40] G. Gradenigo, A. Sarracino, D. Villamaina, T. S. Grigera, and A. Puglisi, J. Stat. Mech. (2010) L12002.

[41] A. Plati and A. Puglisi, Sci. Rep. **11**, 14206 (2021).
[42] M. van den Broek, R. Eichhorn, and C. V. den Broeck, Europhys. Lett. **86**, 30002 (2009).
[43] K. V. Kumar, S. Ramaswamy, and M. Rao, Phys. Rev. E **77**, 020102(R) (2008).
[44] R. Bartussek, P. Hänggi, and J. G. Kissner, Europhys. Lett. **28**, 459 (1994).
[45] A. C. Barato and U. Seifert, Phys. Rev. Lett. **114**, 158101 (2015).
[46] J. M. Horowitz and T. R. Gingrich, Nat. Phys. **16**, 15 (2020).